Annals of Nuclear Energy 112 (2018) 1–8

Contents lists available at ScienceDirect

Annals of Nuclear Energy

journal homepage: www.elsevier.com/locate/anucene

# Rapid radionuclide identification algorithm based on the discrete cosine transform and BP neural network

Jianping He [a], Xiaobin Tang [a,b,*], Pin Gong [a], Peng Wang [a], Liangsheng Wen [a], Xi Huang [a], Zhenyang Han [a], Wen Yan [a], Le Gao [a]

[a] Department of Nuclear Science & Engineering, Nanjing University of Aeronautics and Astronautics, Nanjing, China
[b] Jiangsu Key Laboratory of Nuclear Energy Equipment Materials Engineering, Nanjing, China

ARTICLE INFO

*Article history:*
Received 23 March 2017
Received in revised form 9 June 2017
Accepted 17 September 2017

*Keywords:*
Discrete cosine transform
BP neural network
Feature extraction
Radionuclide identification
Detection rate

ABSTRACT

Traditional radionuclide identification algorithm based on peak detection cannot recognize radioactive material in a short time. This study proposes a rapid radionuclide identification algorithm based on the discrete cosine transform and error back propagation neural network. Detection rate and accurate radionuclide identification distance were used to evaluate the proposed method. Experimental results show that the extracted feature vector of the spectrum is not influenced by time, activity, and distance. The proposed algorithm obtained better results in a relatively authentic environment, and it has the ability to predict the isotopic compositions of the mixed spectrum. The proposed method has a better identification performance for the spectrum of radionuclide masked by shielding material except the gamma rays emitted by related radionuclide are significantly shielded. It is also particularly recommended for the fast radionuclide identification of spectroscopic radiation portal monitors, radioisotope identification devices, and other radiation monitoring instruments.



## 1. Introduction

Radiation monitors are operated at checkpoints (e.g., borders and seaports) to detect and identify radioactive materials in a short time, as well as combat the illegal transportation of radionuclides (Bobin et al., 2016). However, no evident peaks in the gamma spectrum are observed during this short period. Difficulties can arise when the traditional method is used for fast radionuclide identification in this condition.

Artificial neural networks (ANNs) are mathematical models that emulate several of the observed properties of biological nervous systems and draw on the analogies of adaptive biological learning (Kangas et al., 2008). ANNs have been applied in gamma-ray spectrometry analysis (Medhat, 2012; Dragović and Onjia, 2005; Dragović et al., 2005; Dragović et al., 2006). Feature extraction is the kernel step of pattern recognition. Several previous studies have examined aspects of this topic in recent years. For example, Pilato et al. (1999) developed a new method for activity measurement by extracting the principal components of the gamma spectrum by singular value decomposition. However, the said researchers did not utilize it for radionuclide identification. Chen and Wei (2009) proposed a radionuclide identification method based on the Karhunen–Loeve transform (KLT) and neural network (NN), but the measuring time was approximately 1 min. Contrary to the traditional method, calibration, peak detection, and deconvolution are not required when utilizing NNs to analyze the gamma spectrum.

The present study proposes a novel rapid radionuclide identification algorithm based on the discrete cosine transform (DCT) and error back propagation (BP) NN. Experiments on different source types, time, activities, distances, number of radionuclide, and gamma-ray shielding were performed to verify the radionuclide identification performance of the proposed method.

## 2. Methods and experiments

The proposed algorithm is composed of background subtraction, feature extraction, and radionuclide identification. Fig. 1 shows the procedure of the proposed algorithm. First, the background and radionuclide spectra are both smoothed by wavelet decomposition. The subtraction spectrum is then obtained by subtracting the portion of the smoothed background spectrum according to the ratio of the radionuclide scan time to the background scan time. Second, the DCT is performed on the subtraction

* Corresponding author at: Department of Nuclear Science & Engineering, Nanjing University of Aeronautics and Astronautics, Nanjing, China.
*E-mail address:* tangxiaobin@nuaa.edu.cn (X. Tang).

https://doi.org/10.1016/j.anucene.2017.09.032
0306-4549/

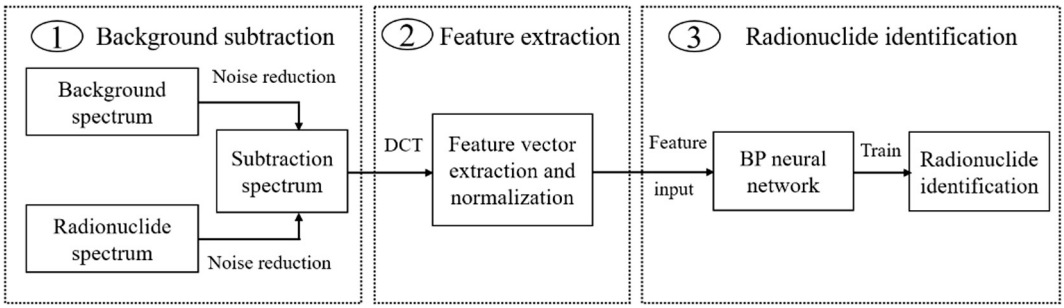


**Fig. 1.** Block diagram of the proposed algorithm.

spectrum to obtain the transformed spectrum. A certain number of transform coefficients is selected as the feature vector in the transformed spectrum. Finally, the normalized feature vector is inputted into the NN, and the trained NN is applied to predict the isotopic compositions of the spectrum.

### 2.1. Feature extraction

DCT is an orthogonal transformation method (Ahmed et al., 1974), and its transform kernel is a cosine function as shown in Eq. (1). It is often considered as the optimized transform of the speech and image signals, and its transform kernel is changeless, which only depends on the dimensions of data. The signal of transformed spectrum is mainly concentrated in the low frequency region, which provides a new way for feature extraction. DCT is a promising method for transforming the gamma spectrum. The spectrum can be seen as a vector $y$ with the dimension of $N$, and then $y(x)$ ($x = 0, 1, 2, 3 \ldots N-1$) is a form of discrete signal of the spectrum. Therefore, the spectrum can be expressed as Eq. (2) after DCT. Given that the signal of the $Y(u)$ spectrum is mainly concentrated in the low frequency region, more than 90% energy of the original spectrum can be reserved by selecting a small amount of transform coefficients in that region. The selected transform coefficients can be seen as spectrum features and are adopted as inputs for the NN. Thus,

$$t(x,u) = C(u)\sqrt{\frac{2}{N}}\cos\frac{(2x+1)u\pi}{2N} \quad C(u) = \begin{cases} \frac{1}{\sqrt{2}} & u = 0 \\ 1 & other \end{cases} \tag{1}$$

where $u$ is an integer, that is, in the range of 0 to $N-1$.

$$Y(u) = C(u)\sqrt{\frac{2}{N}}\sum_{x=0}^{N-1} y(x)\cos\frac{(2x+1)u\pi}{2N} \quad (u,x = 0,1,2\ldots N-1) \tag{2}$$

### 2.2. BPNN model

The BPNN is a multilayer feedforward NN that is trained by the BP algorithm. It is composed of input, hidden, and output layers (Yoshida et al., 2002). Each layer includes neurons that are connected to all the neurons of the succeeding layer. Weight, $w_{ij}$, exists for each connection between the two neurons, $i$ and $j$. The neuron sums up all the signals it receives; each signal is multiplied by its associated weights on the connection, and the sum of the weights is processed with a certain activation function. This process describes the signal transmission in the NN. The initial weights of ANNs are often selected randomly by an algorithm, which can cause errors between the output and the target (actual). The BP algorithm works by minimizing the error through propagating it back into the network. The weights on each of the connections between the neurons are changed according to the error size. The training is stopped when the root mean square error (RMSE) reaches an acceptable value. For machine learning, the key step is feature extraction, which can be completed by feature transform (e.g., KLT, DCT, singular value decomposition (SVD), fast fourier transform (FFT), etc.). BPNN may have better performance if we can extract the main feature of spectrum.

In the present study, 128 transform coefficients were selected as feature vectors of the spectrum; thus, the number of input neurons is 128. The number of hidden neurons is set at 8 according to the empirical Eq. (3). $^{238}$Pu, $^{131}$I, $^{60}$Co, and $^{137}$Cs are used to verify the proposed method, thus, the number of output neurons is 4. Each output indicates whether a radionuclide exists in the environment or not. Fig. 2 shows the BPNN model used.

$$k = \log_2 m \tag{3}$$

where $m$ is the number of input neurons, and $k$ is the number of hidden neurons.

### 2.3. Performance evaluation of the proposed method

In order to evaluate the proposed method, gamma ray spectrometry system which consists of 3″ × 3″ NaI (Tl) detector (ORTEC Inc.) coupled with a PC-based multichannel analyzer (MCA) (ORTEC Inc.) along with MAESTRO software installed in the PC was used, and MAESTRO 7.01 (ORTEC Inc.) software was used to obtain the spectra. The energy of this detector ranges from 30 keV to 3000 keV, and the resolution is approximately 7.7% (at 662 keV). The detector was installed at a fixed location, and the radionuclides were placed at points A, B,..., I in 20-cm intervals as shown in Fig. 3. Samples with different times, activities, and distances were obtained. The background spectrum without any source was collected for 300 s to generate the background template. Table 1 lists the radionuclides utilized in the experiment. They are labeled as Nucl-1, Nucl-2, Nucl-3, Nucl-4, Nucl-5, Nucl-6, Nucl-7, and Nucl-8 for convenience of description. The net count of each radionuclide measured at point A (Fig. 3) with detection time of 10 s was given, and the count of background with detection time of 10 s was also given. The dose rate of background without adding shielding apparatus was measured in the laboratory (about 0.1 μSv/h).

The detection rate was used to evaluate the identification performance of the proposed algorithm. The detection rate is defined by the ratio of the correctly identified data to the total amount of data as shown in Eq. (4) (Min et al., 2012):

$$Detection\ rate(\%) = \frac{TP + TN}{TP + TN + FP + FN} \times 100 \tag{4}$$

where $TP$ is true positive, $TN$ is true negative, $FP$ is false positive, and $FN$ is false negative.

The accurate radionuclide identification distance (ARID) of each radionuclide was calculated from the detection rate results with

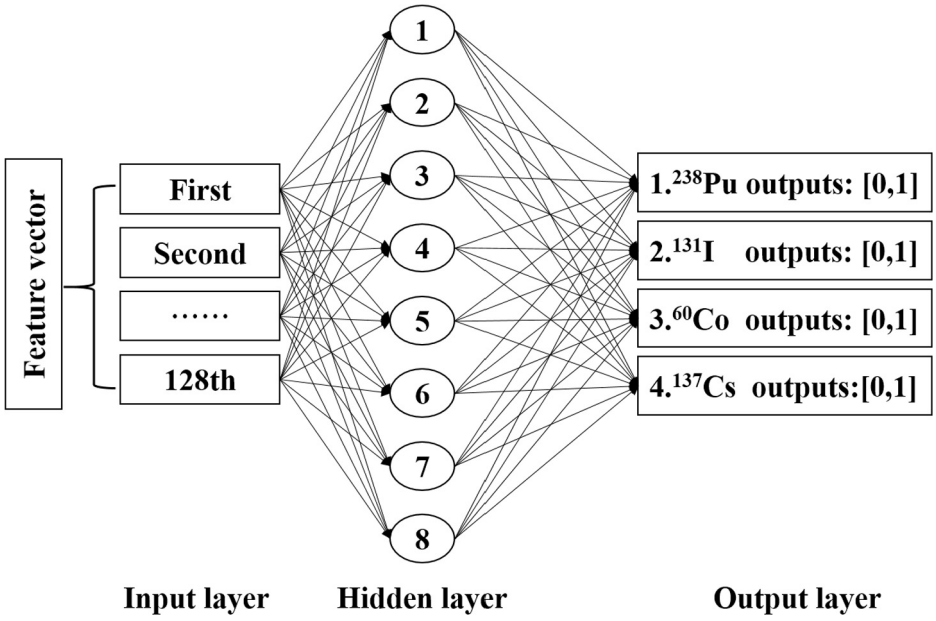


**Fig. 2.** Structure of the BPNN adopted in this study.

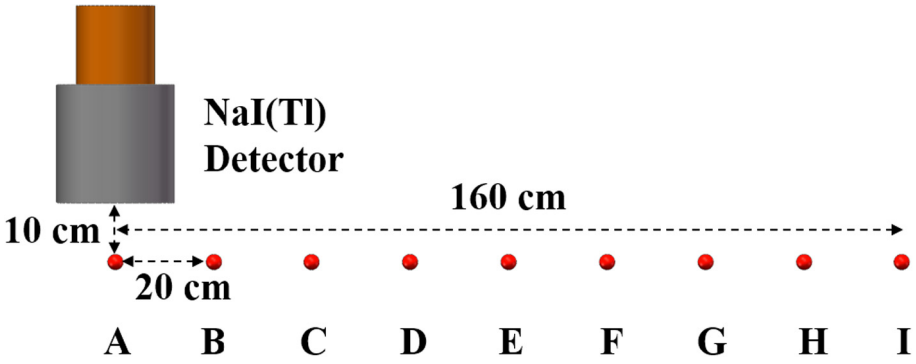


**Fig. 3.** Schematic of the experimental environment.

**Table 1**
Radionuclides for the experiments conducted in this study.

| Radionuclide | $^{238}$Pu | $^{238}$Pu | $^{131}$I | $^{131}$I | $^{60}$Co | $^{60}$Co | $^{137}$Cs | $^{137}$Cs |
|---|---|---|---|---|---|---|---|---|
| Label | Nucl-1 | Nucl-2 | Nucl-3 | Nucl-4 | Nucl-5 | Nucl-6 | Nucl-7 | Nucl-8 |
| Activity (μCi) | $8.95 \times 10^3$ | $8.92 \times 10^3$ | 6 | 30.5 | 1.67 | 1.67 | 1.27 | 1.43 |
| Count (10 s) | 4342 | 3482 | 7139 | 11989 | 13429 | 13485 | 5731 | 6296 |
| Background | 5552 | 5552 | 5552 | 5552 | 5552 | 5552 | 5552 | 5552 |

respect to the distance of the source to the detector (Min et al., 2014). The ARID is the maximum distance at which detection rates are guaranteed to be reliably above the required level. The detection rate of the acceptance level in this study is 98.3% as recommended by the ANSI N42.35 standard (Ansi, 2007).

### 2.4. Description of the spectra used in this study

#### 2.4.1. Acquisition of the training samples

The NN must be trained by proper samples. The spectra of eight different combinations (i.e., Nucl-1, Nucl-3, Nucl-5, Nucl-7, Nucl-1 + Nucl-5, Nucl-1 + Nucl-7, Nucl-5 + Nucl-7, and Nucl-1 + Nucl-5 + Nucl-7) measured at point A were obtained. The measurement was repeated 10 times for each condition, and the measuring time was 10 s. For example, the measurement for Nucl-1 + Nucl-5 with monitoring point at A and scan time of 10 s would be repeated 10 times. The same rulers apply to other combinations. Thus, 80 spectra were obtained. We proportionately selected 60% of these spectra as training samples, whereas the remaining 40% were used as verifying samples.

#### 2.4.2. Acquisition of samples at different times, activities, and distances

The spectra of Nucl-1, Nucl-3, Nucl-5, and Nucl-7 measured at point A were obtained to explore the time effect on the radionuclide identification performance of the proposed algorithm. The measurement was repeated 10 times for each condition, and the measuring times were 4, 6, and 8 s. A total of 120 spectra were obtained, which were all used as testing samples.

The spectra of Nucl-1 + Nucl-2, Nucl-4, Nucl-5 + Nucl-6, and Nucl-7 + Nucl-8 measured at point A were obtained to explore

the activity effect on the radionuclide identification performance of the proposed algorithm. The measurement was repeated 10 times for each condition, and the measuring times were 4, 6, 8, and 10 s. Thus, 160 spectra were obtained, which were all used as testing samples.

The spectra of Nucl-1, Nucl-4, Nucl-5, and Nucl-7 measured from points B to I at 20-cm intervals were obtained to explore the effect of distance on the radionuclide identification performance of the proposed algorithm. The measurement was repeated 10 times for each condition, and the measuring time was 10 s. Hence, 320 spectra were obtained, which were all used as testing samples.

*2.4.3. Acquisition of samples for the stability analysis of feature extraction*

A validation program is required to analyze the stability of feature extraction. The feature vector of the $^{60}$Co spectrum was analyzed to simplify the validation program. The Nucl-5 spectrum with the monitoring point at A and scan time of 4 s; Nucl-5 spectrum with the monitoring point at A and scan time of 10 s; Nucl-5 spectrum with the monitoring point at B and scan time of 10 s; and Nucl-5 + Nucl-6 spectrum with the monitoring point at A and scan time of 10 s are selected for the stability analysis of feature extraction.

*2.4.4. Acquisition of moving radionuclide samples*

A simulation experiment was designed to verify the radionuclide identification performance of the proposed algorithm in a real environment. By assuming that Nucl-1, Nucl-5, and Nucl-7 placed at point I approach point A along the line segment IA at a speed of 0.1 m/s, which is the speed mentioned in a related article (Boardman et al., 2012), the spectrum when radionuclides arrived at each monitoring point was obtained. The spectrum at 2 s in each monitoring point was obtained to simulate the radionuclides that have speeds of 0.1 m/s. A total of 8 spectra with scan times from 2 s to 16 s in 2-s intervals were obtained.

*2.4.5. Acquisition of samples of different number of radionuclide, and gamma-ray shielding*

The spectra of seven different combinations (i.e., Nucl-1, Nucl-5, Nucl-7, Nucl-1 + Nucl-5, Nucl-1 + Nucl-7, Nucl-5 + Nucl-7, and Nucl-1 + Nucl-5 + Nucl-7) measured at point A (Fig. 3) were obtained to explore the effect of number of radionuclide on the proposed method. The measurement was repeated 10 times for each condition, and the measuring time was 4 s. For example, the measurement for Nucl-1 + Nucl-5 with monitoring point at A and scan time of 4 s would be repeated 10 times. The same rulers apply to other combinations. Thus, 70 spectra were obtained, which were all used as testing samples. Three combinations (i.e., Nucl-1, Nucl-5, and Nucl-7) of seven combinations correspond to the condition with number of radionuclide of value 1; three combinations (i.e., Nucl-1 + Nucl-5, Nucl-1 + Nucl-7, and Nucl-5 + Nucl-7) of seven combinations correspond to the condition with number of radionuclide of value 2; one combination of seven combinations (i.e., Nucl-1 + Nucl-5 + Nucl-7) corresponds to the condition with number of radionuclide of value 3.

The spectra of seven different combinations (i.e., Nucl-1, Nucl-5, Nucl-7, Nucl-1 + Nucl-5, Nucl-1 + Nucl-7, Nucl-5 + Nucl-7, and Nucl-1 + Nucl-5 + Nucl-7) masked by lead (0.2 or 1.0 mm thick) or tin (0.2 or 1.0 mm thick) and measured at point A (Fig. 3) were obtained to explore the effect of gamma-ray shielding on the proposed method. The measurement was repeated 10 times for each condition, and the measuring time was 10 s. Hence, 280 spectra were obtained, which were all used as testing samples. Three combinations (i.e., Nucl-1, Nucl-5, and Nucl-7) of seven combinations correspond to the condition with number of radionuclide of value 1; three combinations (i.e., Nucl-1 + Nucl-5, Nucl-1 + Nucl-7, and Nucl-5 + Nucl-7) of seven combinations correspond to the condition with number of radionuclide of value 2; one combination of seven combinations (i.e., Nucl-1 + Nucl-5 + Nucl-7) corresponds to the condition with number of radionuclide of value 3. Seven different combinations masked by lead of thickness of 0.2 mm, seven different combinations masked by lead of thickness of 1.0 mm, seven different combinations masked by tin of thickness of 0.2 mm, and seven different combinations masked by tin of thickness of 1.0 mm are 4 different experimental setup, and we could obtain 70 spectra in each experimental setup. This is why we could obtain 280 spectra in number.

## 3. Results and discussion

### 3.1. Results of the NN training

A comparative experiment was conducted to demonstrate the advantage of the proposed algorithm, and a new method was developed by replacing the DCT with the KLT as shown in Fig. 1. All of the results are in the same condition. The trained NN must be tested by verifying samples to validate whether it has fully learned the pattern characteristics of the spectra. Table 2 lists the single radionuclide detection rates (%) of the training samples. Two methods can effectively extract the major characteristics of the spectrum because the detection rates of the single radionuclide (i.e., $^{238}$Pu, $^{131}$I, $^{60}$Co, and $^{137}$Cs) reached 100%. Therefore, the NN has fully learned and memorized the pattern characteristics of the spectra of the related radionuclides extracted by the two methods. Thus, the trained NN can predict the isotopic composition of the spectra.

### 3.2. Effects of time, activity, and distance on the proposed method

The time, activity, and distance can change the spectral intensity; therefore, the effects of time, activity, and distance on the radionuclide identification performance of the proposed method must be explored. Table 3 lists the single radionuclide detection rates (%) of the samples at different times. The detection rate of a single radionuclide reaches 100% at different times for the DCT. By contrast, the detection rates of $^{238}$Pu, $^{60}$Co, and $^{137}$Cs are 0% at different times for the KLT. Moreover, only $^{131}$I has a detection rate of 100%. The feature vector was normalized so that the change in spectral intensity does not affect the radionuclide identification performance of the proposed method as shown in Fig. 1. The feature vector extracted by KLT was also normalized, but similar results were not attained. The KLT method reflects the correlation

**Table 2**
Single radionuclide detection rates (%) of the training samples.

| Method | $^{238}$Pu | $^{131}$I | $^{60}$Co | $^{137}$Cs |
|---|---|---|---|---|
| DCT | 100 | 100 | 100 | 100 |
| KLT | 100 | 100 | 100 | 100 |

**Table 3**
Single radionuclide detection rates (%) of the samples at different times.

| Time | Method | $^{238}$Pu | $^{131}$I | $^{60}$Co | $^{137}$Cs |
|---|---|---|---|---|---|
| 4 s | DCT | 100 | 100 | 100 | 100 |
| | KLT | 0 | 100 | 0 | 0 |
| 6 s | DCT | 100 | 100 | 100 | 100 |
| | KLT | 0 | 100 | 0 | 0 |
| 8 s | DCT | 100 | 100 | 100 | 100 |
| | KLT | 0 | 100 | 0 | 0 |

**Table 4**
Single radionuclide detection rates (%) of the samples at different activities.

| Time | Method | $^{238}$Pu | $^{131}$I | $^{60}$Co | $^{137}$Cs |
|---|---|---|---|---|---|
| 4 s | DCT | 100 | 100 | 100 | 100 |
| | KLT | 0 | 100 | 0 | 0 |
| 6 s | DCT | 100 | 100 | 100 | 100 |
| | KLT | 0 | 100 | 0 | 0 |
| 8 s | DCT | 100 | 100 | 100 | 100 |
| | KLT | 0 | 100 | 0 | 0 |
| 10 s | DCT | 100 | 100 | 100 | 100 |
| | KLT | 0 | 100 | 0 | 0 |

of the channel-to-channel counts through the covariance matrix of the selected sample; therefore, its transform kernel varies with the samples. The correlation of the channel-to-channel counts will change due to the statistical fluctuation of radioactive decay at different times.

Table 4 lists the single radionuclide detection rates (%) of the samples at different activities. The detection rate of the single radionuclide reaches 100% at different activities for the DCT. The change in activity can be attributed to the change in spectral intensity, and the change in spectral intensity is eliminated by the normalization process of the feature vector. The measuring times set as 4, 6, 8, and 10 s have no effect on the proposed algorithm. However, the detection rates of $^{238}$Pu, $^{60}$Co, and $^{137}$Cs are 0% at different activities for the KLT. Moreover, only $^{131}$I has a detection rate of 100%. Given the aforementioned reason, the change in activity can lead to change in the statistical fluctuation of radioactive decay.

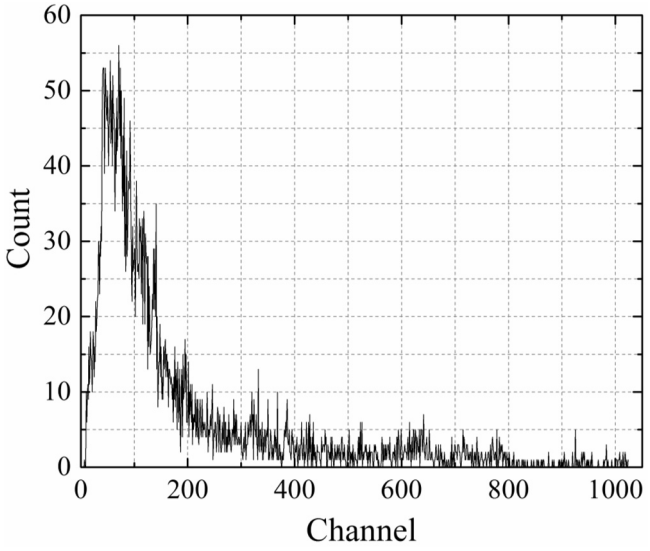


**Fig. 5.** Nucl-5 spectrum with a measuring time of 10 s and source-to-detector distance of 80 cm.

Fig. 4 shows the single radionuclide detection rates (%) of the samples at different distances. This figure shows that the ARID values of $^{238}$Pu, $^{131}$I, $^{60}$Co, and $^{137}$Cs are greater than or equal to 60, 140, 80, and 100 cm for the DCT, respectively. The corresponding minimum detectable activity (MDA) of $^{238}$Pu, $^{131}$I, $^{60}$Co, and $^{137}$Cs are less than or equal to $8.95 \times 10^3$, 30.5, 1.67, and 1.27 μCi, respectively (Gong et al., 2014; Tang et al., 2016). The effect of the dis-

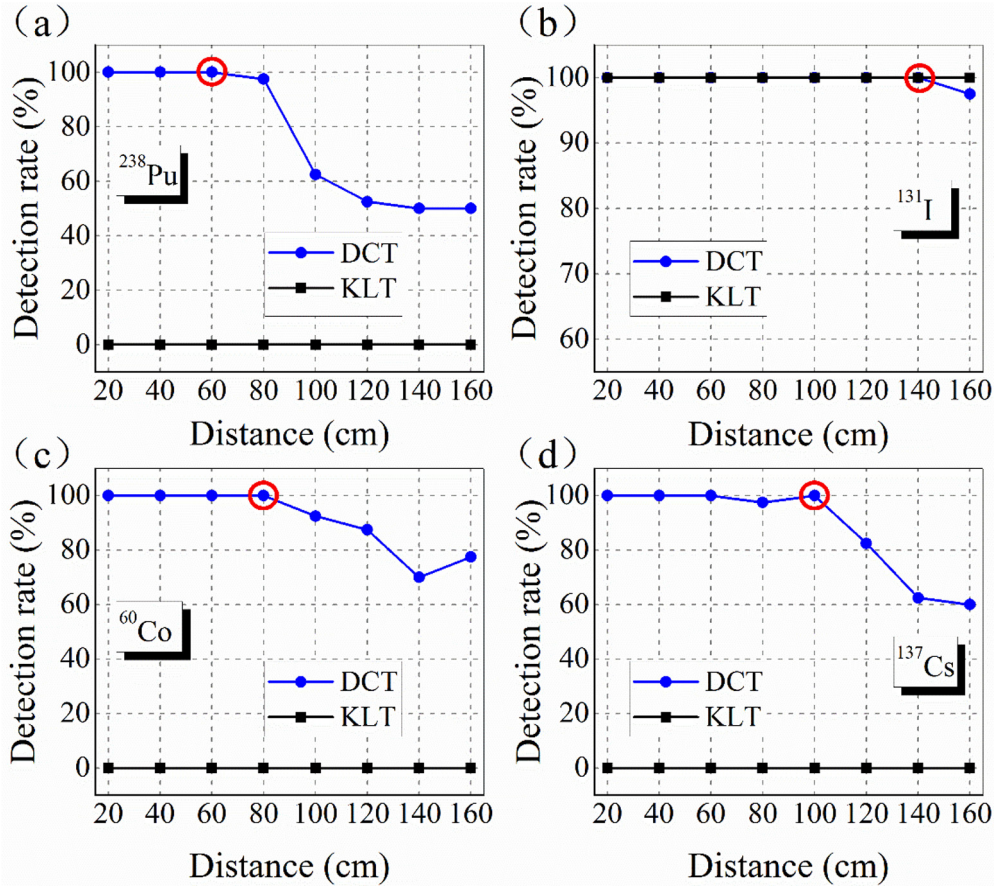


**Fig. 4.** Single radionuclide detection rates (%) of the samples at different distances. (a) $^{238}$Pu, (b) $^{131}$I, (c) $^{60}$Co, and (d) $^{137}$Cs.

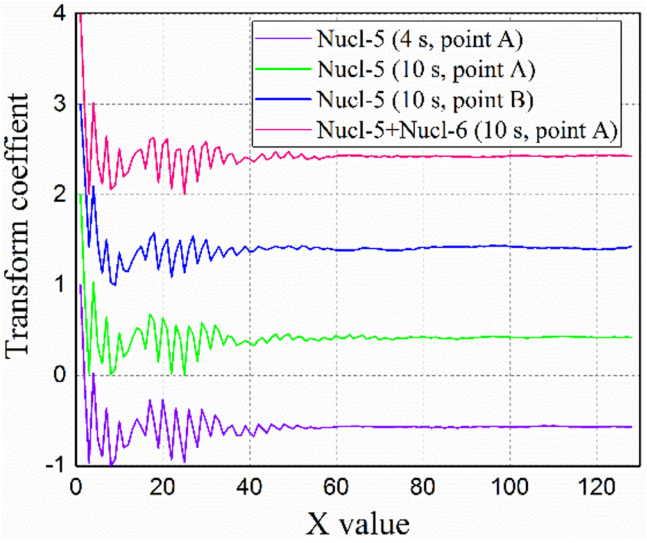


**Fig. 6.** Feature vector chart of the sample for the stability analysis of feature extraction.

tance between the source and the detector can also be attributed to the change in spectral intensity. By contrast, the ARID values of $^{238}$Pu, $^{60}$Co, and $^{137}$Cs are 0 cm for the KLT; only $^{131}$I has an ARID value larger than or equal to 160 cm. These results are attributed to the changes in the detection distance, which can also cause the variation in the statistical fluctuation of radioactive decay.

The Nucl-5 spectrum with a measuring time of 10 s and source-to-detector distance of 80 cm is shown in Fig. 5 to reflect the radionuclide identification performance of the proposed algorithm more intuitively. The signal-to-noise ratio (SNR) is extremely low in this scenario, and the characteristic peaks of the $^{60}$Co cannot be observed at all. However, the $^{60}$Co is identified by the proposed algorithm with a detection rate of 100%, which reflects the advantage of the proposed method over the traditional method.

### 3.3. Effects of time, activity, and distance on the stability of feature extraction

The extracted feature vector of the spectrum must not vary with time, activity, and distance. Otherwise, the NN cannot easily converge with the global minimum. Fig. 6 shows the feature vector chart of the sample for the stability analysis of feature extraction. Three curves are shifted upward by 1, 2, and 3 units to observe the results conveniently. Although the measurement times, activities, and detection distances are different, the feature vector of the spectrum of the same radionuclide exhibits a coincidence trend after normalization. Therefore, the extracted feature vector of the spectrum is the same as the "ID" of the radionuclide.

### 3.4. Comprehensive experiment

Radionuclides generally move at a certain velocity in real conditions, which can affect the radionuclide identification performance of the proposed method. Table 5 lists the results in the real environment. Only $^{60}$Co is identified from point H to point C; $^{238}$Pu and $^{60}$Co are both identified at point B; $^{238}$Pu, $^{60}$Co, and $^{137}$Cs are all identified at point A; and the identification status of $^{131}$I is always "*N*" from point H to point A. Thus, all the radionuclides are identified correctly, and no errors occurred in the entire process. Results show that the proposed algorithm can be utilized for fast radionuclide identification in a real environment, and it is a relatively robust radionuclide identification algorithm. Fig. 7 shows the synthetic spectra of three radionuclides (i.e., Nucl-1 + Nucl-5 + Nucl-7) at points H, B, and A.

### 3.5. Effects of different number of radionuclide, and gamma-ray shielding

The spectral shape of radionuclide would change when adding another radionuclide to it, and sometimes the peaks are overlapped for multiple radionuclides with similar energy, which poses a challenge to the proposed method. Table 6 lists the results of samples at different number of radionuclide. The single radionuclide detection rate of $^{238}$Pu, $^{60}$Co, and $^{137}$Cs are all 100% at different number of radionuclide, which indicates the proposed method are not affected by the number of radionuclide and it has the ability to predict the isotopic compositions of the mixed spectrum. The main reason is that the feature vector of spectrum of multiple radionuclides is extracted by the DCT and learned by the BPNN.

As we know, the radiation intensity will decrease in an exponential fashion with the thickness of the absorber with rate of decrease being controlled by the linear attenuation coefficient. So the effect of gamma-ray shielding on the proposed method should be studied. Table 7 shows that the single radionuclide detection rate of $^{60}$Co, and $^{137}$Cs are 100% when the value of number of radionuclide is 1, but the single radionuclide detection rate of $^{238}$Pu is only 90%. This is due to the scattering effect of shielding materials and a few of samples are identified as which contains$^{137}$Cs when only $^{238}$Pu exists in the environment, though the proposed method has a positive response for $^{238}$Pu in this process. Both the $^{60}$Co and $^{137}$Cs are properly identified when the value of number of radionuclide is 2 or 3, but the $^{238}$Pu can't be recognized, which is due to the compton scattering of $^{60}$Co or $^{137}$Cs with higher energy than $^{238}$Pu.

Table 8 shows that the single radionuclide detection rate of $^{60}$Co, and $^{137}$Cs are 100% when the value of number of radionuclide is 1, but the single radionuclide detection rate of $^{238}$Pu is only 85%, which is due to the increase of thickness of lead and only part of samples are properly identified when only $^{238}$Pu exists in the environment. Both the $^{60}$Co and $^{137}$Cs are identified correctly when the value of number of radionuclide is 2 or 3, but the $^{238}$Pu can't be recognized for the same reasons as already mentioned.

Tables 9 and 10 show that both the $^{60}$Co and $^{137}$Cs are properly identified when the value of number of radionuclide is 1, 2, or 3, and the $^{238}$Pu can't be recognized. This is due to the fact that only tin with thickness of 0.2 mm can shield most of gamma rays emitted by $^{238}$Pu, but tin with thickness of 1 mm can only shield part of gamma rays emitted by $^{60}$Co or $^{137}$Cs. Above all, the proposed method has a better identification performance for the spectrum

**Table 5**
Sample results in a real environment.

| Point | H | G | F | E | D | C | B | A |
|---|---|---|---|---|---|---|---|---|
| $^{238}$Pu | N | N | N | N | N | N | P | P |
| $^{131}$I | N | N | N | N | N | N | N | N |
| $^{60}$Co | P | P | P | P | P | P | P | P |
| $^{137}$Cs | N | N | N | N | N | N | N | P |

Note: *N* (negative) and *P* (positive) indicate the absence and presence of radionuclides.

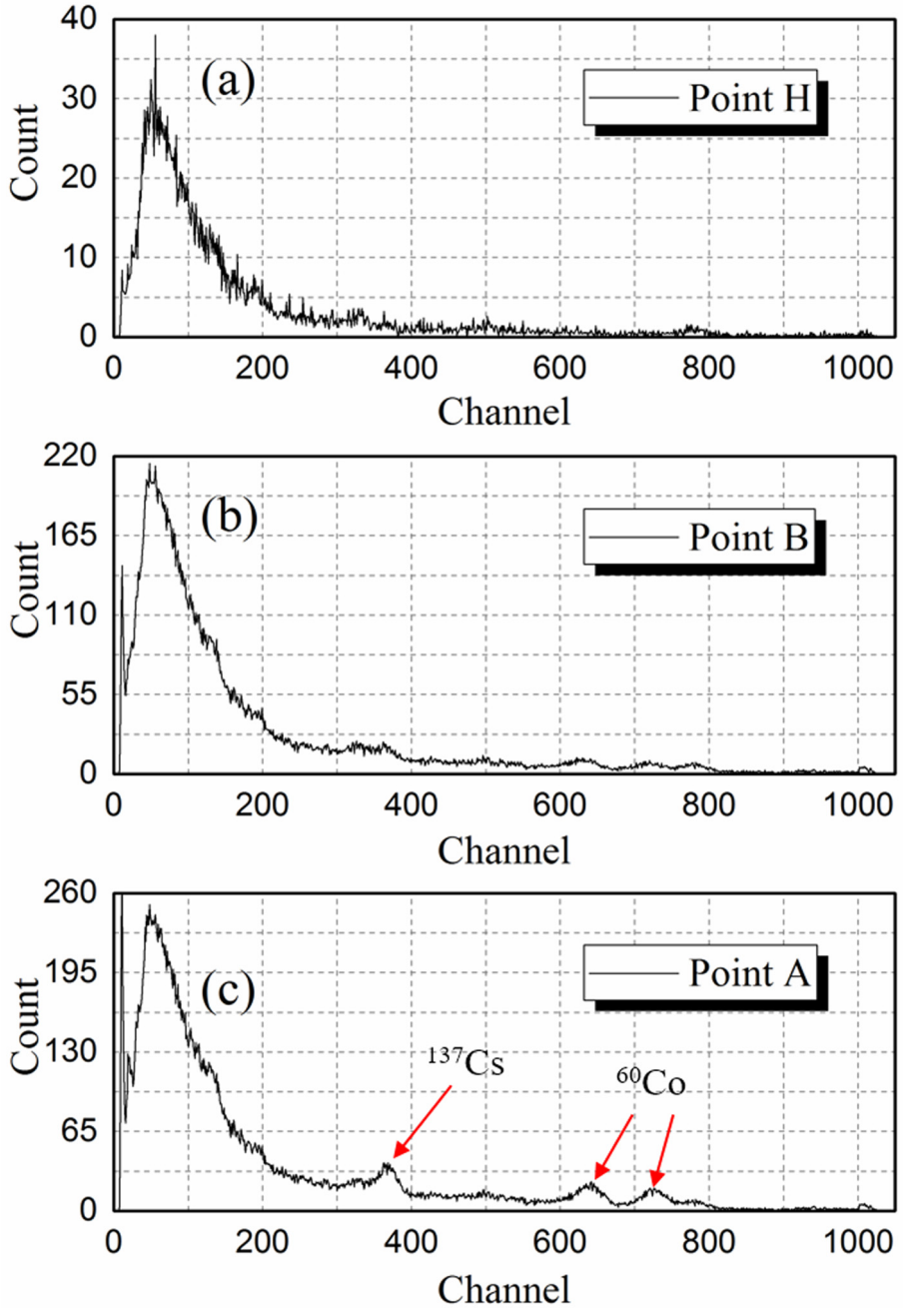


**Fig. 7.** Synthetic spectra of three radionuclides (i.e., Nucl-1 + Nucl-5 + Nucl-7) at (a) Point H, (b) Point B, and (c) Point A.

**Table 6**
Single radionuclide detection rates (%) of the samples at different number of radionuclide.

| Number of radionuclide | $^{238}$Pu | $^{60}$Co | $^{137}$Cs |
|---|---|---|---|
| 1 | 100 | 100 | 100 |
| 2 | 100 | 100 | 100 |
| 3 | 100 | 100 | 100 |

**Table 7**
Single radionuclide detection rates (%) of the samples with radionuclides masked by lead with thickness of 0.2 mm.

| Number of radionuclide | $^{238}$Pu | $^{60}$Co | $^{137}$Cs |
|---|---|---|---|
| 1 | 90 | 100 | 100 |
| 2 | 75 | 87.5 | 87.5 |
| 3 | 75 | 75 | 75 |

**Table 8**
Single radionuclide detection rates (%) of the samples with radionuclides masked by lead with thickness of 1 mm.

| Number of radionuclide | $^{238}$Pu | $^{60}$Co | $^{137}$Cs |
|---|---|---|---|
| 1 | 85 | 100 | 100 |
| 2 | 75 | 87.5 | 87.5 |
| 3 | 75 | 75 | 75 |

**Table 9**
Single radionuclide detection rates (%) of the samples with radionuclides masked by tin with thickness of 0.2 mm.

| Number of radionuclide | $^{238}$Pu | $^{60}$Co | $^{137}$Cs |
|---|---|---|---|
| 1 | 75 | 100 | 100 |
| 2 | 75 | 87.5 | 87.5 |
| 3 | 75 | 75 | 75 |

**Table 10**
Single radionuclide detection rates (%) of the samples with radionuclides masked by tin with thickness of 1 mm.

| Number of radionuclide | $^{238}$Pu | $^{60}$Co | $^{137}$Cs |
|---|---|---|---|
| 1 | 77.5 | 100 | 100 |
| 2 | 75 | 87.5 | 87.5 |
| 3 | 75 | 75 | 75 |

of radionuclide masked by shielding material except the gamma rays emitted by related radionuclide are significantly shielded.

## 4. Conclusion

This study develops a rapid radionuclide identification algorithm based on the DCT and BPNN. This algorithm is composed of background subtraction, feature extraction, and radionuclide identification. The effects of noise and background radiation are effectively eliminated by background subtraction. Moreover, the feature vector of the spectrum is extracted by the DCT method. Finally, the isotopic composition of the spectrum is identified by the trained BPNN.

Experimental results show that the radionuclide identification performance of the proposed method is not affected by time, activity, distance, and number of radionuclide as long as the MDA of a single radionuclide is met. The radionuclides used in this study is $^{238}$Pu ($8.89 \times 10^3$ and $8.92 \times 10^3$ μCi), $^{131}$I (6 and 30.5 μCi), $^{60}$Co (1.67 and 1.67 μCi), and $^{137}$Cs (1.27 and 1.43 μCi), and the dose rate of background without adding shielding apparatus was measured in the laboratory (about 0.1 μSv/h). the proposed method has a better identification performance for the spectrum of radionuclide masked by shielding material except the gamma rays emitted by related radionuclide are significantly shielded. The extracted feature vector of the spectrum is the same as the "ID" of the radionuclide. Furthermore, the proposed method can also correctly identify all radionuclides that appear in the experimental setup without making errors in the comprehensive experiment. The radionuclide identification algorithm based on KLT and NN cannot obtain better results under the same training conditions. However, the KLT removes the correlation of the original signals, reverses the maximum energy, and minimizes the mean square error; thus, it is also called the optimized transform. The proposed algorithm can only identify the trained radionuclides, and an error response to the untrained radionuclides may occur. The detection rates of radionuclides will decrease gradually, whereas the false identifying rate will increase with decreasing SNR. The MDA of a single radionuclide must also be met.

Further work, such as determining the optimal number of hidden neurons and using genetic algorithm to optimize the BP NN, will be performed to improve the radionuclide identification performance of the proposed method. The proposed method is particularly suitable for the fast radionuclide identification of spectroscopic radiation portal monitors, radioisotope identification devices, and other radiation monitoring instruments. This algorithm can be executed in mobile or embedded system for the trained BPNN is not complicated and it requires less execution times. In this study, the algorithm is executed in windows based mini PC.

## Acknowledgments

This work was supported by the National Natural Science Foundation of China (Grant No. 11675078), the Foundation of Graduate Innovation Center in NUAA (Grant Nos. kfjj20160606; kfjj20170613; kfjj20170617) and the Fundamental Research Funds for the Central Universities, the Primary Research and Development Plan of Jiansu Province (Grant No. BE2017729), the Fundamental Research Funds for the Central Universities (Grant No. NJ20160034), the Funding of Jiangsu Innovation Program for Graduate Education (Grant No. KYLX16_0353) and the Fundamental Research Funds for the Central Universities, and the Priority Academic Program Development of Jiangsu Higher Education Institutions.

## References

Ahmed, N., Natarajan, T., Rao, K.R., 1974. Discrete cosine transform. IEEE. Trans. Comput. C 23 (1), 90–93.
Ansi, N., 2007. American National Standard for Evaluation and Performance of Radiation Detection Portal Monitors for Use in Homeland Security. ANSI N42.35-2006. c1-35.
Boardman, D., Reinhard, M., Flynn, A., 2012. Principal component analysis of gamma-ray spectra for radiation portal monitors. IEEE. Trans. Nucl. Sci. 59 (1), 154–160.
Bobin, C., Bichler, O., Lourenço, V., Thiam, C., Thévenin, M., 2016. Real-time radionuclide identification in γ-emitter mixtures based on spiking neural network. Appl. Radiat. Isot. 109, 405–409.
Chen, L., Wei, Y.X., 2009. Nuclide identification algorithm based on K-L transform and neural networks. Nucl. Instrum. Methods Phys. Res. A. 598, 450–453.
Dragović, S., Onjia, A., 2005. Prediction of peak-to-background ratio in gamma-ray spectrometry using simplex optimized artificial neural network. Appl. Radiat. Isot. 63, 363–366.
Dragović, S., Onjia, A., Stanković, S., Aničin, I., Bačić, G., 2005. Artificial neural network modelling of uncertainty in gamma-ray spectrometry. Nucl. Instrum. Methods Phys. Res. A. 540, 455–463.
Dragović, S., Onjia, A., Bačić, G., 2006. Simplex optimization of artificial neural networks for the prediction of minimum detectable activity in gamma-ray spectrometry. Nucl. Instrum. Methods Phys. Res. A. 564, 308–314.
Gong, C.H., Zeng, G.Q., Ge, L.Q., Tang, X.B., Tan, C.J., 2014. Minimum detectable activity for NaI(Tl) airborne γ-ray spectrometry based on Monte Carlo simulation. Sci. Chi. Technol. Sci. 57, 1840–1845.
Kangas, L.J., Keller, P.E., Siciliano, E.R., Kouzes, R.T., Ely, J.H., 2008. The use of artificial neural networks in PVT-based radiation portal monitors. Nucl. Instrum. Methods Phys. Res. A. 587, 398–412.
Medhat, M.E., 2012. Artificial intelligence methods applied for quantitative analysis of natural radioactive sources. Ann. Nucl. Energ. 45, 73–79.
Min, E., Ko, M., Kim, Y., Joung, J., Lee, K., 2012. A Peak Detection in Noisy Spectrum Using Principal Component Analysis. Nucl. Sci. Symp. Med. Imaging. Confer. Record (NSS/MIC). 2012 IEEE, 62–65.
Min, E., Ko, M., Lee, H., Kim, Y., Joung, J., Joo, S.K., Lee, K., 2014. Identification of radionuclides for the spectroscopic radiation portal monitor for pedestrian screening under a low signal-to-noise ratio condition. Nucl. Instrum. Methods Phys. Res. A. 758, 62–68.
Pilato, V., Tola, F., Martinez, J.M., Huver, M., 1999. Application of neural networks to quantitative spectrometry analysis. Nucl. Instrum. Methods Phys. Res. A. 422, 423–427.
Tang, X.B., Meng, J., Wang, P., Cao, Y., Huang, X., Wen, L.S., Chen, D., 2016. Simulated minimum detectable activity concentration (MDAC) for a real-time UAV airborne radioactivity monitoring system with HPGe and LaBr 3 detectors. Radiat. Meas. 85, 126–133.
Yoshida, E., Shizumaa, K., Endo, S., Oka, T., 2002. Application of neural networks for the analysis of gamma-ray spectrums measured with a Ge spectrometer. Nucl. Instrum. Methods Phys. Res. A. 484, 557–563.